Comparative pathogenesis of two lineages of Powassan virus reveals differing routes of neuroinvasion leading to distinct clinical outcome, neuropathology and inflammation.

Erin S. Reynolds[1,2,3], Charles E. Hart[4], Jacob T. Nelson[1,2,3], Brandon J. Marzullo[5,6], Allen T. Esterly[7], Dakota N. Paine[1,2,3], Jessica Crooker[1,2,3], Paul T. Massa[1,8], Saravanan Thangamani[1,2,3]

[1] Department of Microbiology and Immunology, SUNY Upstate Medical University, Syracuse, New York, USA

[2] SUNY Center for Vector-Borne Diseases, SUNY Upstate Medical University, Syracuse, New York, USA

[3] Institute for Global Health and Translational Science, SUNY Upstate Medical University, Syracuse, New York, USA

[4] Molecular Biology Section, Laboratory Sciences Directorate, Defense Centers for Public Health Aberdeen, Aberdeen Proving Grounds, MD, USA

[5] Department of Biochemistry, Jacobs School of Medicine and Biomedical Sciences, SUNY Buffalo, Buffalo, New York, USA

[6] Genomics and Bioinformatics Core, New York State Center of Excellence Bioinformatics & Life Sciences, SUNY Buffalo, Buffalo, New York, USA

[7] Section of Infectious Diseases, Department of Internal Medicine, Yale School of Medicine, New Haven, CT, USA

20 [8] Department of Neurology, SUNY Upstate Medical University, Syracuse, New York, USA

21 **Abstract**

22 Tick-borne flaviviruses (TBFV) can cause severe neuroinvasive disease which may result in death
23 or long-term neurological deficit in over 50% of survivors. Multiple mechanisms for invasion of
24 the central nervous system (CNS) by flaviviruses have been proposed including axonal
25 transport, transcytosis, endothelial infection, and Trojan horse routes. Flaviviruses may utilize
26 different or multiple mechanisms of neuroinvasion depending on the specific virus, infection
27 site, and host variability. In this work we have shown that infection of BALB/cJ mice with either
28 Powassan virus lineage I (Powassan virus) or lineage II (Deer tick virus) results in distinct spatial
29 tropism of infection in the CNS which correlated with unique clinical presentation for each
30 lineage. Comparative transcriptomics of infected brains demonstrates activation of different
31 immune pathways and suggests that in this model CNS invasion occurs via transport into the
32 spinal cord and brain stem during Powassan virus infection rather than through forebrain
33 structures in Deer tick virus infection. These results implicate distinct modes of neuroinvasion
34 into and dissemination within the CNS that ultimately dictate the differential pathogenesis of
35 these clinically important emerging viruses.

36 **Author Summary**

37 Powassan virus causes a nationally notifiable disease which can cause severe neurological
38 disease in humans and has no approved vaccines or therapeutics. Although two distinct
39 lineages circulate in North America, clinical differentiation is not typically performed, and
40 pathology has been assumed to be similar between lineages. In this work, a direct comparison

41 of lineage I (Powassan virus) and lineage II (Deer tick virus) demonstrated distinct differences in
42 the clinical presentation, pathology of the central nervous system, and immune response in
43 immunocompetent mice. These differences suggest that Deer tick virus and Powassan virus do
44 not utilize the same mechanisms for neuroinvasion and dissemination within the CNS. This is
45 clinically relevant as the development of treatment plans and therapeutics need to be
46 evaluated for these virus lineages.

47 **Introduction**

48 Powassan virus is the only known TBFV circulating in North America and has two distinct
49 genetic lineages. Prototypical Powassan virus, lineage I (POWV), was isolated in 1958 and
50 known to be vectored by *Ixodes cookei* ticks (1,2). Lineage II Powassan virus is also known as
51 Deer tick virus (DTV) and was initially isolated in 1995 and is vectored primarily by *Ixodes*
52 *scapularis* ticks (3,4). Powassan virus and DTV share approximately 84% nucleotide sequence
53 identity and 94% amino acid identity but are serologically indistinguishable (5–8). The number
54 of cases and geographic range for both POWV and DTV have increased, coinciding with the
55 expansion of *Ixodes* tick and increased surveillance. In addition, recent studies have
56 demonstrated that Powassan lineages may not only be vectored by *Ixodes* ticks but may also be
57 transmitted by some species of *Dermacentor*, *Amblyomma*, and *Haemaphysalis* ticks (9–11).

58 Infection with POWV is usually asymptomatic; however, some individuals will experience a
59 febrile illness that can progress to severe neuroinvasive disease that may present with
60 meningoencephalitis or paralysis. Case fatality rates are estimated to be between 10% to 15%,
61 and over 50% of POWV survivors experience long-term neurological sequelae (5,12). While

62 there have been advances in the study of POWV neuroinvasive disease, the underlying
63 pathology is not completely defined, especially in relation to the similarly pathogenic DTV.
64 Powassan virus disease is a nationally notifiable condition but differentiation of lineages is not
65 required (13). When lineage differentiation is performed for human cases it is most often done
66 through sequencing of viral RNA as methods such as neutralization and immunohistochemistry
67 use antibodies which are cross reactive (14–17).

68 The neuropathology seen in POWV is currently believed to be mediated by a combination of
69 inflammatory cytokines breaching the integrity of the blood-brain barrier (BBB) and
70 intravasating leukocytes. Of possible relevance to differential POWV and DTV pathogenesis,
71 infections by clinically important TBFV may provide important clues on what determines
72 particular disease outcomes. For instance, the levels of TNFα, IL-1β, IL-6, and IL-8 have been
73 associated with the proinflammatory breakdown of the BBB through the loss of tight junctions,
74 with MMP-9 being crucial for neuroinvasive disease with tick-borne encephalitis virus (TBEV)
75 (18,19). Once the integrity of the BBB has been compromised, the cellular destruction and
76 pathology associated with TBEV infection are driven by the migration of CD8+ T-lymphocytes
77 and NK cells (20). Besides immune-mediated neuronal destruction, neuronal demise can occur
78 throughout the CNS with deficits related to the area in the brain damaged, as evidenced by
79 mapping a neuronal network with brains infected by the related Langat virus (LGTV) (21).
80 Noting the differences in CNS pathogenesis of TBFV, we describe here essential differences in
81 the pathogenicity of POWV and DTV which are of relevance as historically they were assumed
82 to be interchangeable, which makes these findings novel and clinically relevant. As such, we

83 propose that the present studies support a reconsideration of distinct pathogenetic outcomes
84 of infection by POWV lineages in humans.

85 **Results**

86 **Immunocompetent mice inoculated with DTV and POWV had different clinical disease**
87 **presentations.**

88 We investigated whether equivalent doses of either DTV or POWV resulted in a different clinical
89 presentation in six-week-old BALB/cJ mice. The first outward signs of illness occurred at 5 days
90 post infection (dpi) when weight loss was observed in both infected groups (Fig. 1A, B).
91 Although weight loss occurred across both infected groups, it was more severe in the DTV-
92 infected mice (Fig. 1B). Seventy-five percent of DTV-infected mice (n=9) and 8% of POWV-
93 infected mice (n=1) reached loss of 20% or greater from their baseline weight and required
94 humane euthanasia (Fig. 1D). Starting at 6dpi generalized signs of febrile illness occurred in
95 both groups including ruffled coat, hunched posture, lethargy, and rapid or labored respiration.
96 Ocular discharge and closure of one or both eyes occurred in both infected groups between
97 6dpi and 8dpi but was more common in DTV-infected mice (50%, n=6) than POWV-infected
98 mice (33%, n=4.) Onset of neurological illness occurred at 6dpi in the POWV infected mice and
99 at 7dpi for the DTV infected mice and was markedly different between groups. Forty-two
100 percent of DTV-infected mice presented with neurological illness, including seizure (n=4) (Fig.
101 1D) and weak grip which progressed to paralysis (n=1) (Fig. 1D). In contrast, neurological illness
102 was present in 83% POWV-infected mice, with 25% mice exhibiting multiple signs. Observed

103 signs in POWV-infected mice included weak grip (n=3), paresis (n=3), loss of righting
104 reflex/prostration (n=2), seizure (n=1), and paralysis (n=5) (Fig. 1D).

105 Mean clinical disease scores and percent weight change from baseline were compared between
106 all groups until 8dpi, after which sample sizes were too small for statistical comparison, using
107 one-way ANOVA with Šídák's multiple comparisons test. Between 5dpi and 8dpi, there were
108 statistically significant differences in the clinical disease scores between uninfected mice and
109 each infected group and between DTV and POWV infected mice at the second daily
110 observations on 6dpi [p=0.0404] and 7dpi [p=0.001] (Fig. 1A). Body weight changes from
111 baseline were significantly different between uninfected and each infected group starting at
112 6dpi but not between DTV and POWV infected groups (Fig. 1B).

113 Differences in mean clinical disease scores and percent weight change from baseline were also
114 compared between male and female mice within a group using a two-tailed Student's t-test.
115 The DTV infected male and female mice had significantly different clinical scores during the first
116 daily observation at 7dpi [p=0.0298] (Fig. S1A) and no significant differences were found in the
117 POWV infected male and female mice (Fig. S1F). In addition, trends in weight loss were
118 consistent between male and female DTV and POWV infected mice (Fig. S1B, G). Overall, DTV
119 infected mice experienced a higher degree of weight loss than POWV infected mice while
120 POWV infected mice experienced more loss of ambulation than DTV infected mice.

121 **Immunocompetent mice inoculated with DTV and POWV had the same time to death.**

122 Despite differences in clinical disease, all mice inoculated via footpad with 10^3 FFU of DTV or
123 POWV succumbed to disease between 6 and 11 dpi. Log-rank test (Mantel-Cox) did not show

124 significant differences in survival between DTV and POWV infected mice (Fig. 1C), which had
125 median survival times (MST) of 7.5 and 7 days, respectively. In addition, no significant
126 differences were present between male and female mice within a group (Fig. S1C, H) using the
127 same analyses. MST for DTV-infected mice were 7 days for males and 8.5 days for females,
128 while MST for POWV-infected mice were 7 days for both males and females.

129 **Viral titers differ in blood and tissues of DTV and POWV infected mice.**

130 Viral RNA was detected in blood samples from all DTV-infected mice and all except one POWV-
131 infected mouse between 1dpi and 3dpi (Fig. 1E). Viral RNA declined following 3dpi and was not
132 detected in blood samples after 9dpi. Mean viremia for the DTV group peaked on 2dpi at 1.798
133 Log FFU/µg RNA equivalents, while the POWV group peaked on 1dpi at 2.258 Log FFU/µg RNA
134 equivalents (Fig. 1E). At 1dpi, there was higher viremia in POWV-infected mice than in DTV-
135 infected mice [p=0.0314] using a two-tailed Student's t-test with Welch's correction.

136 Detection of viral RNA in organs demonstrated that DTV and POWV disseminate throughout the
137 body. Viral RNA was present in the brain, popliteal lymph node from the injected leg, spleen,
138 and lung of all infected mice (Fig. 1F). There was viral RNA detected in the heart and kidney of
139 all DTV-infected mice and 92% POWV-infected mice (n=11.) Viral RNA was present at the
140 injection site for 50% of the mice in each infected group (n=6.) Limited viral RNA was found in
141 the liver with either no viral RNA or RNA below the detection limit in 92% DTV-infected mice
142 (n=11) and 67% POWV-infected mice (n=8.)

143 The highest amounts of viral RNA were detected in the brains of both infected groups, with an
144 average of 7.43 Log FFU/µg RNA equivalents present in the DTV group and 5.62 Log FFU/µg

145 RNA equivalents present in the POWV group (Fig. 1F). The brains of DTV-infected mice had
146 higher viral loads than POWV-infected mice [p=0.0096], while the POWV-infected mice had
147 higher viral loads in the lymph node [p=0.0002.] A comparison of viral RNA present in organs
148 was also performed between infected male and female mice and the only significant difference
149 was found in the livers of POWV-infected mice (Fig. S1I). All analyses were performed by a two-
150 tailed Student's t-test with Welch's correction.

151 **Comparative Histopathology of Deer Tick Virus and Powassan Virus Infected Brains and Spinal**
152 **Cords.**

153 Histopathological changes were observed in POWV and DTV infected mouse brains across
154 multiple regions including the olfactory bulb (OB), cerebral cortex (CTX), hippocampal
155 formation (HPF), hypothalamus (HY), thalamus (TH), midbrain (MB), pons (P), medulla (MY),
156 and cerebellum (Purkinje layer: CB – P, granular layer: CB- G, molecular layer: CB – M) and
157 scored by severity (Table S2). Infected mice exhibited microgliosis and neuronal necrosis in the
158 cerebellum (Fig. 2A-C) and olfactory bulb (Fig. 2J-L), degenerating neurons and vacuolation of
159 neuropil were observed Ammon's horn of the hippocampal formation (Fig. 2D-F), and the
160 isocortex showed perivascular cuffing and meningoencephalitis (Fig. 2G-I). Lesion severity
161 scores were averaged and compared using two-tailed Student's t-test with Welch's correction.
162 Deer tick virus infected mice had higher lesion severity scores in the HPF, TH, and MB regions
163 compared to POWV infected mice (Fig. 3A, B).
164 Powassan virus infected brains showed meningoencephalitis (Fig. 2I) that had progressed into
165 the cervical spinal cord (Fig. 4C), while the meninges of the spinal cord appeared normal in DTV
166 infected samples (Fig. 4B). Cervical spinal cords of POWV infected mice exhibited considerable

167 histopathology in which nuclei of ventral gray matter motoneurons were either shrunken with
168 irregular cell bodies or had entirely degenerated (Fig. 4F). There was also conspicuous
169 extravasation of inflammatory cells in spinal cord gray matter of POWV infected mice,
170 especially in the cervical spinal cord (Fig. 4C, F, I, L). In contrast, neurons in the cerebellum and
171 spinal cord of DTV infected mice appeared normal in numbers and morphology (Fig. 2B, Fig. 4B,
172 E).
173 Brain sections stained for viral RNA and CD11b+ cells were examined and scored by severity in a
174 manner consistent with histopathological analysis (Table S3). Powassan virus and DTV infection
175 of neurons were noted throughout all infected animal brains; however, the regions infected
176 differed between viruses. The brains infected with POWV exhibited staining of viral RNA in all
177 regions but were concentrated primarily in the cerebellum and brainstem (Fig. 5C). Powassan
178 virus only rarely infected the hippocampus, isocortex, and olfactory bulb in most animals (Fig.
179 5G, H, K, L) compared to relatively high levels of infection of Purkinje cells and granule cells in in
180 the cerebellum (Fig. 5C).

181 Deer tick virus-infected brains showed a markedly different pattern of viral infection. There
182 was reduced infection in the cerebellum and brainstem (Fig. 5A, B) in comparison to POWV
183 infected brains but a pronounced increase of viral RNA found in neurons in the isocortex,
184 olfactory bulb, and hippocampal formation including the dentate gyrus granule cells and
185 pyramidal neurons in Ammon's horn (Fig. 5E, F, I, J). Virus severity scores show increased virus
186 in the CTX, HPF, and TH of DTV infected mice and increased virus in the CB of POWV infected
187 mice (Fig. 6A, B). CD11b severity scores show an increased positive cells in the HPF of DTV-
188 compared to POWV- infected mice (Fig. 6C).

189 Neuron specific staining differed in the spinal cords of POWV and DTV infected mice. In DTV
190 infected mice minimal viral RNA was present across the cervical, thoracic, and lumbar regions
191 (Fig. 7B, E, H, K). Prominent infection of cervical spinal cord neurons of POWV infected mice
192 was consistent with contiguous brainstem, cerebellum and midbrain regions that were also
193 positive for POWV. The presence of viral RNA-containing neurons decreased considerably from
194 cervical to thoracic and lumbar regions in several animals indicating that the cervical spinal cord
195 was particularly affected at this stage of infection (Fig. 7C, F, I, L). One POWV-infected mouse
196 had prominent infection of the hippocampus and isocortex (Table S3) however, this animal also
197 had the characteristic lower brain stem and spinal cord infection seen in the other POWV-
198 infected mice.

199 In summary, infection of the brainstem, cerebellum, and contiguous cervical spinal cord by
200 POWV correlates with the observed clinical signs seen during POWV infection, in which animals
201 exhibited substantial paralysis and motor deficits while infection with DTV was concentrated
202 mainly to the cerebral cortex, olfactory bulbs, and midbrain with less lower brainstem and
203 spinal cord involvement. The distinct regional patterns of infection by DTV and POWV are
204 depicted schematically in Fig. 6B.

205 **Comparative Transcriptomics of POWV and DTV**

206 Transcripts from either DTV or POWV-infected brains were generated and compared against
207 the uninfected controls and represented increased levels of inflammatory cytokine and
208 chemokine genes (Fig. S3A, B; Fig. S4). The smallest p-adjusted value for either group was
209 STAT1, with genes involved in immunological signaling, inflammation, and interferon response

210 following infection (Fig. S3C, D). The 25 genes with the smallest p-values in POWV-infected
211 brains are involved with interferon signaling, antigen presentation and viral response (Fig. S6 C,
212 D). There was a significant upregulation in genes responsible for controlling viral infection in
213 both samples, including interferon-stimulated genes and innate immune signaling genes
214 associated with MyD88 and RIG-I like receptors. Individually, both POWV and DTV appear to
215 activate the JAK-STAT pathway through TLR stimulation and interferon production producing an
216 anti-viral state.

217 The transcript libraries generated from POWV- and DTV-infected brains were then compared
218 (Fig. 8A) and smaller libraries were generated based on GO enrichment analysis terms:
219 inflammatory response (Fig. 8B), immune system process (Fig. 8C), and defense response (Fig.
220 8D). The brain tissues infected with POWV had significantly higher levels of inflammatory
221 pathway genes including NLRP6 and chemokines associated with hematopoietic inflammatory
222 cell recruitment including CX3CR1. The tissues infected with DTV displayed higher levels of
223 Cav1, which induces NF-κB through T-cell activation. Furthermore, there is a strong difference
224 in the levels of CXCL3, with DTV-infected tissues having significantly higher levels of the
225 neutrophil chemotactic cytokine. The results from this comparison suggest that while there is a
226 similar pattern to the interferon response and establishment of the anti-viral state, DTV and
227 POWV infections of the CNS involve the recruitment of different cell types and activation of
228 different inflammatory pathways.

229 **Cytokine and chemokine analysis of terminal serum.**

230 Levels of 23 analytes were measured in terminal blood serum and evaluated using Brown-
231 Forsythe and Welch's ANOVA with Dunnett's T3 multiple comparisons test to determine
232 differences in means between uninfected (n=12), DTV infected (n=11), and POWV infected
233 (n=8) mice (Fig. S2). There were significantly higher levels of six analytes in DTV-infected groups
234 compared to uninfected groups: IL-10 [p=0.0321], IL-12(p40) [p=0.006], MCP-1 [p=0.031], MIP-
235 1α [p=0.0059], MIP-1β [p=0.0237], and RANTES [p=<0.0001]. In contrast, there were only
236 significantly lower levels in four analytes in POWV-infected animals compared to controls: GM-
237 CSF [p=0.0112], IL-1 [p=0.0249], IL-5 [p=0.0121], and IL-13 [p=0.0004]. The only difference
238 between DTV and POWV was in IL-13 [p=0.0451]. These data indicate an entirely different
239 proinflammatory response in the periphery following infection by these two viruses.

240 **Discussion**

241 Flaviviruses are endemic across much of the globe and cause millions of cases of human illness
242 each year (22). Severity of neurotropic flaviviruses such as West Nile virus (WNV), Japanese
243 encephalitis virus (JEV), TBEV, and Powassan virus can range from mild to fatal and can cause
244 severe neuroinvasive disease with long-term sequelae in a high percentage of survivors. For
245 example, disease severity, fatality rate, and long-term sequelae associated with TBEV infection
246 has been shown to vary depending on the subtype despite the high sequence similarity
247 between these viruses (23,24). Similarly, DTV and POWV share approximately 94% amino acid
248 identity and 84% nucleotide sequence similarity and are serologically indistinguishable (6–8).
249 Coupled with the lack of a vaccine or approved treatment and overlapping circulation in the
250 United States, testing to differentiate lineages is typically not performed for human cases.

251 **Immunocompetent mice inoculated with Powassan virus and Deer tick virus have different**
252 **clinical disease presentations.**

253 In this report, we have shown that DTV and POWV do not have the same clinical presentation
254 when inoculated via the same route and dosage. Common clinical signs in both virus groups
255 included ruffled fur, hunched posture, ocular discharge, and weight loss. The degree of weight
256 loss experienced by DTV-infected mice was more severe than POWV-infected mice. Seizure was
257 the most common neurological symptom present in DTV-infected mice and was consistent with
258 prominent infection and inflammation in the hippocampus. Mice infected with POWV
259 experienced neurological signs more consistent with infection and inflammation of the lower
260 brainstem, cerebellum and spinal cord including paresis and paralysis.

261 **Powassan virus and Deer tick virus induce neuronal death in differing regions of the brain.**

262 The reduced levels of $CD11b^{+}$ cells seen in the histopathology of POWV-infected brains as
263 compared to the DTV-infected brains are congruent with the histopathology and spatial
264 distribution of the virus. The spatial distribution of POWV in the brain is concentrated in the
265 lower brain and spinal cord, while DTV preferentially infected and induced inflammation in the
266 hippocampus and isocortices, which suggests a different neuroinvasive route and/or spread of
267 infection in the brain. The neurologic clinical signs exhibited during late-stage infections are
268 dissimilar as well with DTV eliciting seizures while POWV neuropathology is manifested as
269 motor deficits. The comparative neuropathology of POWV and DTV reveals a stark contrast
270 which is recapitulated in chemokines, histopathology, and observed clinical signs; DTV infects
271 the hippocampus and isocortex, while POWV infection is concentrated within the cerebellum,

272 brain stem, and spinal cord. Interestingly, acute seizures have been linked to loss of the
273 pyramidal cell layer and neuronal loss in the hippocampus in Theiler's murine
274 encephalomyelitis virus-infected mice, which is consistent with pathology findings for mice that
275 experienced seizures in DTV-infected mice in the present work (25,26). Published human cases
276 of fatal DTV infection have shown severe inflammation and infection of the cerebellum and
277 brainstem which is more consistent with neuropathology present in POWV-infected mice
278 (14,15). In these human cases limb weakness and difficulty ambulating were noted and are
279 consistent with the deficits we observed with mice with heavy infection in the cerebellum,
280 brainstem, and cervical spinal cord.

281 Changes in the clinical presentation of disease and pattern of infection in the CNS could be
282 attributed to a variety of factors, including person-to-person variability, site of infection, and
283 genomic diversity of viruses. Other flaviviruses have demonstrated that genetic diversity in the
284 E and NS5 regions change the phenotype of the virus including immunogenicity and
285 pathogenicity (27). The strain of POWV or DTV used for inoculation, route and method of
286 inoculation and time spent replicating in the periphery could affect the clinical signs and
287 response to infection (21,23,28–30). This is underscored by our findings in that the vectored
288 route of inoculation can cause a diverse set of clinical signs but ultimately be relegated to either
289 a cortical region meningoencephalitis or involve the cerebellum and spinal cord, resulting in
290 descending myelitis.

291 **Host Chemokine and Inflammatory Response to Powassan virus is different compared to Deer**
292 **tick virus.**

293 Neuroinvasion of flaviviruses has been shown to be a result of inflammatory breakdown of the
294 blood-brain barrier; however, other mechanisms may result in CNS infection as well. Our
295 findings are consistent with previous studies showing an upregulation of STAT1 and genes
296 associated with inflammation and interferon in the brain of moribund animals. The
297 histopathological differences seen between the regions of the brain infected by DTV and POWV
298 suggest a spatial tropism which may be affected by a region-specific neuroinvasion and
299 dissemination. The olfactory bulb of DTV-infected animals had high levels of virus present
300 which suggests that this area was significant for viral replication and consequent spreading to
301 cerebral cortex and to the underlying midbrain structures. The clinical signs in POWV-infected
302 animals combined with the histopathology clearly show myelitis and destruction of neurons in
303 the ventral horns of the cervical spinal cord, contiguous lower brain stem, and cerebellum,
304 illustrating a differing spatial tropism compared to DTV. The differences in these spatial
305 tropisms could be explained by differential routes of neuroinvasion, with DTV for instance
306 preferentially crossing the cribiform plate from olfactory neurons to infect the olfactory bulb,
307 while POWV may utilize retrograde axonal transport of virus from the periphery into the spinal
308 cord by the neural route or perhaps by a unique viremic route initiated by preferential
309 inflammatory degradation of the BBB in the spinal cord.

310 The comparative RNA-seq data suggests that there are different innate immune pathways
311 responding to DTV and POWV during CNS infection. While both viruses elicit a strong
312 interferon response, there is a significant increase in NLRP6 and IL1α transcripts in tissues
313 infected with POWV relative to tissues infected with DTV. There is also a significant increase in
314 CX3CR1 and AIRE genes which indicate the recruitment of CD8+ T-cells in POWV infected

315 tissues. The DTV-infected tissues conversely exhibit significant increases in CXCL3 CD177 and
316 CAV1, suggesting neutrophilic recruitment combined with T-cell dependent NF-κB transcription.
317 The spatial tropism exhibited in the histopathology is supported by the levels of Krt6a seen in
318 DTV-infected tissues, which exhibit anti-microbial properties in the olfactory bulb, an area with
319 extensive DTV infection. These findings suggest that the pathology seen in POWV is driven by
320 CD8+ cytotoxic T-lymphocytes, while DTV elicits repetitive NF-κB-mediated transcription and
321 inflammation. These findings are congruent with recent studies that suggest POWV is less
322 inflammatory in neuronal cell cultures and that the pathogenesis of POWV, like TBEV, is driven
323 by the extravasation of cytotoxic T-lymphocytes (20,31). The response to POWV has recently
324 been expanded with experiments examining the role of TRIM5 in POWV infection (32). We
325 have also noted in this report that TRIM5 is upregulated in both DTV and POWV infection
326 compared to uninfected controls; however, TRIM5 is also significantly upregulated in response
327 to POWV as contrasted to the response to DTV infection. This comparative view of RNA
328 transcriptomics in DTV and POWV infection illustrates a difference in cellular and inflammatory
329 response to infection.

330 In conclusion, a direct comparison of POWV (lineage I) and DTV (lineage II) demonstrated
331 distinct differences in clinical presentation and neuro-immunopathology. These differences
332 suggest these two viral lineages do not utilize the same routes of neuroinvasion and stimulate
333 distinct neuroimmunological responses.

334 **Methods**

335 **Ethics Statement**

336 Mouse experiments were conducted in an American Association for the Accreditation of
337 Laboratory Animal Care (AAALAC) approved facility within Animal Biosafety Level 3 (ABSL3)
338 containment. All procedures were performed in accordance with SUNY Upstate Medical
339 University Institutional Animal Care and Use Committee approved protocol (#455) which
340 adhered to the Guide for the Care and Use of Laboratory Animals (33).

341 **Animals, viruses, and infection**

342 Thirty-six 5-week-old male (n=18) and female (n=18) BALB/cJ mice were purchased from The
343 Jackson Laboratory (Bar Harbor, ME). Upon receipt, mice were housed three per cage in
344 individually ventilated cages with HEPA-filtered supply and exhaust air. Food and water were
345 provided *ad libitum*. Animals were provided a 12h light/12h dark cycle within a temperature
346 and humidity-controlled room. Mice were acclimated to the facilities for one week. On the day
347 of study initiation, prior to infection, animals were observed and weighed to ensure there were
348 no apparent physical abnormalities and that each group had a similar weight distribution.
349 Uninfected control mice had an average weight of 21.43g (± 2.09), DTV-infected mice had an
350 average weight of 20.74g (± 1.98), and POWV-infected mice had an average weight of 21.06g (±
351 2.16).

352 All mice received a single footpad injection of 30µL under isoflurane anesthesia. Control mice
353 received serum-free Dulbecco's Modified Eagle Medium (DMEM, Corning), and infected mice
354 received 10^3 focus forming units (FFU) of either POWV Lineage I (POWV LB) or Lineage II (DTV
355 Spooner). Each group contained six male and six female mice. These numbers were selected to
356 provide the minimum number of animals required to determine statistical significance between

357 sexes within a treatment group. Bodyweight measurements and detailed clinical observations
358 were performed daily to assess the animal appearance, behavior, respiration, and neurological
359 signs of disease (Table S1). Submandibular blood collection was performed from Days 0 to 7
360 using alternating cohorts of mice and alternating sites. Terminal blood was collected via cardiac
361 puncture following euthanasia.

362 When animals reached the criteria for humane euthanasia or at 11 days post-infection (dpi)
363 euthanasia was performed by CO_2 inhalation followed by cervical dislocation. Whole body
364 perfusion was performed using 10mL of sterile 0.9% sodium chloride, USP. Tissues collected at
365 necropsy were stored in either Buffer RLT (Qiagen) or 10% Neutral Buffered Formalin (NBF).
366 Blood was stored in Buffer RLT. Samples stored in Buffer RLT were maintained in ABSL3 facilities
367 for a minimum of 24 hours to allow inactivation. Samples stored in 10% NBF were fixed for a
368 minimum of 72 hours, with one change of NBF occurring 24 hours after collection.

369 No specific methods were used to minimize confounders or blind staff to group allocation
370 during the experiment. Each day procedures were performed with uninfected animals handled
371 first, followed by DTV-infected animals, and POWV-infected animals handled last. Equipment
372 and PPE were cleaned or changed between infected groups to prevent cross-contamination.

373 **Viral RNA detection via RT-qPCR**

374 Total RNA was extracted from blood and tissue samples using RNeasy Mini Kits (Qiagen) using
375 previously established modifications to the kit protocol (34). RNA was quantified using a DS-11+
376 Spectrophotometer (Denovix) and tested for the presence of viral RNA by RT-qPCR on a Bio-Rad
377 CFX96 Touch Real-Time PCR System. Viral RNA was detected with forward

378 (CCGAGCCARRGTGAGGATGT), reverse (TCTTTTGCYGARCTCCACTT), and probe
379 (TTCATAGCGAAGGTKAGRTCCAACG) primers which have been previously validated to detect a
380 region of the NS5 gene conserved between POWV and DTV (35). Standard curves for POWV and
381 DTV were generated from 10-fold dilutions of a known quantity of viral RNA and used to
382 estimate viral burden in experimental samples.

383 **Histology and RNA in situ hybridization**

384 Inactivated tissues were transferred to 70% ethanol and shipped to Histowiz, Inc. for
385 embedding and sectioning. Brains were sectioned at 5µM thickness and mounted on glass
386 slides. Hematoxylin and eosin staining was performed at Histowiz, Inc in accordance with their
387 established methods. RNA in situ hybridization was performed using RNAscope 2.5 HD Duplex
388 kits (catalog 322430, Advanced Cell Diagnostics) per manufacturer recommendations. Brain
389 sections underwent dual staining protocol for POWV positive-sense RNA probe (catalog
390 415641) and *Mus musculus* integrin alpha M/CD11b (catalog 311491) to identify infected cells
391 and innate leukocytes. Spine sections underwent dual staining protocol using the same viral
392 RNA probe used on brain sections and *Mus musculus* RNA binding protein, fox-1 homolog (*C.*
393 *elegans*) 3/NeuN (catalog 481707), to identify infected cells including $NeuN^+$ neurons. All slides
394 were counterstained with a 50% solution of Gill's hematoxylin I. Positive control samples were
395 processed using *Mus musculus* Duplex Ppib and Polr2a (catalog 321651) for process verification.

396 Sagittal brain sections were examined in a rostro-caudal direction, including the olfactory bulb,
397 cerebral cortex, hippocampus, thalamus, hypothalamus, midbrain, pons, medulla oblongata,
398 and Purkinje, granular, and molecular layers of the cerebellum. Microscopic lesions, including

399 microgliosis, perivascular cuffing, and neuronal degeneration were graded as: 0 (absence of
400 lesions); 1 (minimal); 2 (mild); 3 (marked.) The presence of meningitis, encephalitis, and
401 meningoencephalitis were noted as M, E, and ME, respectively. RNAscope stained cells were
402 graded a: 0 (absence of staining); 1 (very few to low); 2 (moderate); 3 (numerous). Areas that
403 were not present were noted as NP.

404 **RNA Sequencing and Bioinformatics**

405 Total RNA was quality checked using an Agilent Fragment Analyzer to assess RNA quality and
406 Qubit Fluorescence (Invitrogen) to measure concentration. RNA libraries (200ng total starting
407 material) were prepared following the Illumina RiboZero Total Stranded RNA library prep kit using
408 the ribosomal removal protocol. Following library preparation, concentration and quality control,
409 final libraries were pooled to 10nM and the concentration of the pool was determined using the
410 QuantaBio Universal qPCR reaction kit. After dilution and denaturing, the pooled library was
411 loaded onto an Illumina NovaSeq6000 (PE100) for sequencing at 250pM as final concentration.
412 Per-cycle base call (BCL) files generated by the Illumina NovaSeq were converted to per-read
413 FASTQ files using bcl2fastq version 2.20.0.422 using default parameters. The quality of the
414 sequencing was reviewed using FastQC version 0.11.6. Detection of potential contamination
415 was done using FastQ Screen version 0.14.1. Finally, FastQC and FastQ Screen quality reports
416 were summarized using MultiQC version 1.9.0.
417 Adapter trimming was not performed. Genomic alignments were performed using HISAT2
418 version 2.2.1 using default parameters. Ensembl reference GRCm38 was used for the reference
419 genome and gene annotation set. Sequence alignments were compressed and sorted into
420 binary alignment map (BAM) files using sam tools version 1.3. Counting of mapped reads for

421 genomic features was performed using Subread feature Counts version 2.0.0 using the
422 parameters -p -s 2 –g gene_name –t exon –Q 60 -B -C, the annotation file specified with –a was
423 the Ensembl GRCm38 reference provided by Illumina's iGenomes. Alignment and feature
424 assignment statistics were summarized using MultiQC.
425 Differentially expressed genes were detected using the Bioconductor package DESeq2 version
426 1.38.1. Significance was set to an adjusted p-value less than or equal to 0.05. DESeq2 tests were
427 run for differential expression using a negative binomial generalized linear models, dispersion
428 estimates, and logarithmic fold changes. DESeq2 calculated log2 fold changes and Wald test p-
429 values as well as performing independent filtering and adjusted for multiple testing using the
430 Benjamini-Hochberg procedure to control the false discovery rate (FDR).
431 Gene ontology analysis was performed using the GOSeq Bioconductor package version 1.50.0.
432 GOSeq performs Gene Ontology analysis while addressing biases present in RNA-seq data not
433 found using other techniques, namely that expected read counts for a transcript are based on
434 both, the gene level of expression, and the length of the transcript. While other tools are
435 commonly used for GO term analysis, they do not account for this effect leading to results that
436 are biased toward GO terms with longer transcripts. The Wallenius approximation used by
437 GOSeq approximate GO term enrichment and calculated p-values for each GO category being
438 overrepresented among genes that were differentially expressed. These p-values were
439 corrected for multiple testing using the Benjamini-Hochberg Procedure.
440 **Cytokine and chemokine analysis of terminal serum**
441 Terminal serum samples were tested in duplicate for cytokine and chemokine levels on a Bio-
442 plex 200 (Bio-Rad) using a Bio-plex Pro Mouse Cytokine 23-plex assay according to kit

443 instructions. Cytokines detected were IL-1α, IL-1β, IL-2, IL-3, IL-4, IL-5, IL-6, IL-9, IL-10, IL-12
444 (p40), IL-12 (p70), IL-13, IL-17A, eotaxin, G-CSF, GM-CSF, IFN-γ, KC, MCP-1 (MCAF), MIP-1α,
445 MIP-1β, RANTES, and TNF-α. Serum was diluted 1:4 in the kit supplied diluent, incubated with
446 cytokine-specific labeled beads and detected with biotinylated antibody and streptavidin-PE.

447 **Statistical analysis**

448 Statistical analysis was conducted with GraphPad Prism software version 9.4.1 (GraphPad.) No
449 data were excluded from the analysis.

450 1. McLean DM, Best JM, Mahalingam S, Chernesky MA, Wilson WE. Powassan Virus: Summer
451 Infection Cycle, 1964. Can Med Assoc J. 1964 Dec 26;91(26):1360–2.

452 2. McLean DM, Donohue WL. Powassan Virus: Isolation of Virus from a Fatal Case of
453 Encephalitis. Can Med Assoc J. 1959 May 1;80(9):708–11.

454 3. Telford SR, Armstrong PM, Katavolos P, Foppa I, Garcia AS, Wilson ML, et al. A new tick-
455 borne encephalitis-like virus infecting New England deer ticks, Ixodes dammini. Emerg
456 Infect Dis. 1997;3(2):165–70.

457 4. Ebel GD, Campbell EN, Goethert HK, Spielman A, Telford SR. Enzootic transmission of deer
458 tick virus in New England and Wisconsin sites. The American Journal of Tropical Medicine
459 and Hygiene. 2000 Jul 1;63(1):36–42.

460 5. Hermance ME, Thangamani S. Powassan Virus: An Emerging Arbovirus of Public Health
461 Concern in North America. Vector Borne Zoonotic Dis. 2017 Jul 1;17(7):453–62.

462 6. Beasley DWC, Suderman MT, Holbrook MR, Barrett ADT. Nucleotide sequencing and
463 serological evidence that the recently recognized deer tick virus is a genotype of Powassan
464 virus. Virus Research. 2001 Nov 5;79(1):81–9.

465 7. Kuno G, Artsob H, Karabatsos N, Tsuchiya KR, Chang GJ. Genomic sequencing of deer tick
466 virus and phylogeny of powassan-related viruses of North America. The American Journal of
467 Tropical Medicine and Hygiene. 2001 Nov 1;65(5):671–6.

468 8. Vogels CBF, Brackney DE, Dupuis AP, Robich RM, Fauver JR, Brito AF, et al. Phylogeographic
469 reconstruction of the emergence and spread of Powassan virus in the northeastern United
470 States. Proceedings of the National Academy of Sciences. 2023 Apr
471 18;120(16):e2218012120.

472 9. Hart C, Hassett E, Vogels CBF, Shapley D, Grubaugh ND, Thangamani S. Powassan Virus
473 Lineage I in Field-Collected Dermacentor variabilis Ticks, New York, USA - Volume 29,
474 Number 2—February 2023 - Emerging Infectious Diseases journal - CDC. [cited 2023 May 4];
475 Available from: https://wwwnc.cdc.gov/eid/article/29/2/22-0410_article

476 10. Raney WR, Herslebs EJ, Langohr IM, Stone MC, Hermance ME. Horizontal and Vertical
477 Transmission of Powassan Virus by the Invasive Asian Longhorned Tick, Haemaphysalis
478 longicornis, Under Laboratory Conditions. Front Cell Infect Microbiol. 2022 Jul 1;12:923914.

479 11. Sharma R, Cozens DW, Armstrong PM, Brackney DE. Vector competence of human-biting
480 ticks Ixodes scapularis, Amblyomma americanum and Dermacentor variabilis for Powassan
481 virus. Parasites Vectors. 2021 Dec;14(1):466.

482 12. Ebel GD. Update on Powassan Virus: Emergence of a North American Tick-Borne Flavivirus.
483 Annual Review of Entomology. 2010;55(1):95–110.

484 13. Clinical Evaluation & Disease | Powassan | CDC [Internet]. 2023 [cited 2023 May 10].
485 Available from: https://www.cdc.gov/powassan/clinicallabeval.html

486 14. Tavakoli NP, Wang H, Dupuis M, Hull R, Ebel GD, Gilmore EJ, et al. Fatal Case of Deer Tick
487 Virus Encephalitis. N Engl J Med. 2009 May 14;360(20):2099–107.

488 15. Normandin E, Solomon IH, Zamirpour S, Lemieux J, Freije CA, Mukerji SS, et al. Powassan
489 Virus Neuropathology and Genomic Diversity in Patients With Fatal Encephalitis. Open
490 Forum Infect Dis [Internet]. 2020 Aug 29 [cited 2020 Nov 6];7(10). Available from:
491 https://www.ncbi.nlm.nih.gov/pmc/articles/PMC7566439/

492 16. Solomon IH, Spera KM, Ryan SL, Helgager J, Andrici J, Zaki SR, et al. Fatal Powassan
493 Encephalitis (Deer Tick Virus, Lineage II) in a Patient With Fever and Orchitis Receiving
494 Rituximab. JAMA Neurology. 2018 Jun 1;75(6):746–50.

495 17. Piantadosi A, Rubin DB, McQuillen DP, Hsu L, Lederer PA, Ashbaugh CD, et al. Emerging
496 Cases of Powassan Virus Encephalitis in New England: Clinical Presentation, Imaging, and
497 Review of the Literature. Clin Infect Dis. 2016 Mar 15;62(6):707–13.

498 18. Fortova A, Hönig V, Salat J, Palus M, Pychova M, Krbkova L, et al. Serum matrix
499 metalloproteinase-9 (MMP-9) as a biomarker in paediatric and adult tick-borne encephalitis
500 patients. Virus Research. 2023 Jan 15;324:199020.

501 19. Palus M, Bílý T, Elsterová J, Langhansová H, Salát J, Vancová M, et al. Infection and injury of
502 human astrocytes by tick-borne encephalitis virus. Journal of General Virology.
503 2014;95(11):2411–26.

504 20. Růžek D, Salát J, Palus M, Gritsun TS, Gould EA, Dyková I, et al. CD8+ T-cells mediate
505 immunopathology in tick-borne encephalitis. Virology. 2009 Feb 5;384(1):1–6.

506 21. Chotiwan N, Rosendal E, Willekens SMA, Schexnaydre E, Nilsson E, Lindqvist R, et al. Type I
507 interferon shapes brain distribution and tropism of tick-borne flavivirus. Nat Commun. 2023
508 Apr 10;14:2007.

509 22. Pierson TC, Diamond MS. The continued threat of emerging flaviviruses. Nat Microbiol.
510 2020 Jun;5(6):796–812.

511 23. Tkachev SE, Babkin IV, Chicherina GS, Kozlova IV, Verkhozina MM, Demina TV, et al. Genetic
512 diversity and geographical distribution of the Siberian subtype of the tick-borne encephalitis
513 virus. Ticks and Tick-borne Diseases. 2020 Mar 1;11(2):101327.

514 24. Lindqvist R, Upadhyay A, Överby AK. Tick-Borne Flaviviruses and the Type I Interferon
515 Response. Viruses [Internet]. 2018 Jun 21 [cited 2019 May 16];10(7). Available from:
516 https://www.ncbi.nlm.nih.gov/pmc/articles/PMC6071234/

517 25. Bröer S, Käufer C, Haist V, Li L, Gerhauser I, Anjum M, et al. Brain inflammation,
518 neurodegeneration and seizure development following picornavirus infection markedly
519 differ among virus and mouse strains and substrains. Experimental Neurology. 2016 May
520 1;279:57–74.

521 26. Stewart KAA, Wilcox KS, Fujinami RS, White HS. Development of Post-infection Epilepsy
522 Following Theiler Virus Infection of C57BL/6 Mice. J Neuropathol Exp Neurol. 2010
523 Dec;69(12):1210–9.

524 27. Davis EH, Beck AS, Li L, White MM, Greenberg MB, Thompson JK, et al. Japanese
525 encephalitis virus live attenuated vaccine strains display altered immunogenicity, virulence
526 and genetic diversity. NPJ Vaccines. 2021 Sep 2;6:112.

527 28. Luethy LN, Erickson AK, Jesudhasan PR, Ikizler M, Dermody TS, Pfeiffer JK. Comparison of
528 three neurotropic viruses reveals differences in viral dissemination to the central nervous
529 system. Virology. 2016 Jan 1;487:1–10.

530 29. de Vries L, Harding AT. Mechanisms of Neuroinvasion and Neuropathogenesis by Pathologic
531 Flaviviruses. Viruses. 2023 Jan 17;15(2):261.

532 30. Tigabu B, Juelich T, Holbrook MR. Comparative analysis of immune responses to Russian
533 spring-summer encephalitis and Omsk hemorrhagic fever viruses in mouse models.
534 Virology. 2010 Dec 5;408(1):57–63.

535 31. Nelson J, Ochoa L, Villareal P, Dunn T, Wu P, Vargas G, et al. Powassan Virus Induces
536 Structural Changes in Human Neuronal Cells In Vitro and Murine Neurons In Vivo.
537 Pathogens. 2022 Oct 21;11(10):1218.

538 32. Chiramel AI, Meyerson NR, McNally KL, Broeckel RM, Montoya VR, Méndez-Solís O, et al.
539 TRIM5α Restricts Flavivirus Replication by Targeting the Viral Protease for Proteasomal
540 Degradation. Cell Reports. 2019 Jun 11;27(11):3269-3283.e6.

33. National Research Council (US) Committee for the Update of the Guide for theCare and Use of Laboratory Animals. Guide for the Care and Use of Laboratory Animals [Internet]. 8th ed. Washington (DC): National Academies Press (US); 2011 [cited 2023 May 11]. (The National Academies Collection: Reports funded by National Institutes of Health). Available from: http://www.ncbi.nlm.nih.gov/books/NBK54050/

34. Hermance ME, Hart CE, Esterly AT, Reynolds ES, Bhaskar JR, Thangamani S. Development of a small animal model for deer tick virus pathogenesis mimicking human clinical outcome. PLoS Negl Trop Dis [Internet]. 2020 Jun 15 [cited 2021 Jan 5];14(6). Available from: https://www.ncbi.nlm.nih.gov/pmc/articles/PMC7316340/

35. Hart CE, Bhaskar JR, Reynolds E, Hermance M, Earl M, Mahoney M, et al. Community engaged tick surveillance and tickMAP as a public health tool to track the emergence of ticks and tick-borne diseases in New York. PLOS Global Public Health. 2022 Jun 27;2(6):e0000215.

Fig. 1. Clinical presentation of DTV and POWV infection. Mice (n = 12 per group) were inoculated via the footpad with 10^3 FFU of media (blue), DTV (green), or POWV (purple) and monitored for signs of disease for up to 11 dpi. (A) Clinical signs of disease were categorized and scored by severity (Table S1). Significant differences in DTV and POWV mice clinical scores occurred at the PM observations on 6dpi and 7dpi. (B) Percent weight change from pre-infection. Comparisons on (A) and (B) were made using one-way ANOVA with Šídák multiple comparisons test. Error bars indicate SEM. (C) Survival of mice across all treatments were evaluated using the Mantel-Cox log-rank test and median survival times (MST) were calculated. (D) Humane euthanasia was performed when mice met specific criteria and are categorized to demonstrate differences between DTV and POWV. (E, F) Blood was collected from alternating cohorts of male (n=3) and female (n=3) mice from 0 to 7dpi and at termination blood and tissues (brain, popliteal lymph node, heart, kidney, liver, injection site, spleen, and lung) were collected from all animals to determine viral loads via rt-qPCR. For brain analysis, six animals

568 per group (3M and 3F) were tested and for all other tissues twelve animals (6M and 6F) were
569 tested. Viral loads are expressed as Log FFU equivalents per microgram of RNA after
570 normalization to a standard curve. Comparisons on (D) and (E) were performed using two-tailed
571 Student's t-test with Welch's correction.

572 **Fig. 2.** Neuropathological examination of DTV and POWV infected mouse brains. Uninfected
573 mouse with normal structures shown in (A) cerebellum with molecular cell layer - M, Purkinje
574 cell layer - P, and granular cell layers - G, (D) Ammon's horn of the hippocampus, (G) isocortex,
575 and (J) olfactory bulb. Cerebella of DTV (B) and POWV (C) infected mice with microgliosis (red
576 arrow) and neuronal cell necrosis (red circle). Ammon's horn of the hippocampus from DTV (E)
577 and POWV (F) infected mice with neuropil vacuolation (red arrow) and hyper eosinophilic
578 degenerating neurons (black arrow). Isocortex of DTV (H) and POWV (I) with infiltration of
579 leptomeninges (black arrow) and perivascular cuffing (red arrow). Olfactory bulb of DTV (K) and
580 POWV (L) infected mice with neuronal cell necrosis in granular cell layers (black arrow).

581 **Fig. 3.** Severity of lesions in DTV and POWV-infected mouse brains by region. (A) Severity of
582 individual mice by region. Comparisons performed using unpaired two-tailed Student's t-test
583 with Welch's correction. (B) Brain regions of DTV infected mice had statistically significant
584 differences in severity in the HPF, MB, and TH regions.

585 **Fig. 4.** Neuropathological examination of DTV and POWV infected mouse spinal cords.
586 Uninfected mouse with normal structures shown in (A, D) cervical region (black arrow shows
587 motor neuron in ventral horn), (G) thoracic region, and (J) lumbar region. DTV infected mouse
588 (B) cervical region, (E) motor neuron (black arrow) in dorsal horn, (H) thoracic region, and (K)
589 lumbar region. POWV infected mouse with (A) meningoencephalitis (red arrow) in cervical

590 region, (F) absent and degenerating motor neuron (black arrow) in dorsal horn, and infiltrations
591 in (I) thoracic and (L) lumbar regions.

592 **Fig. 5.** Divergent patterns of infection in DTV and POWV infected mouse brains. Representative
593 images of DTV infected (A, B, E, F, I, J) and POWV infected (C, D, G, H, K, L) brains stained for
594 viral RNA (teal) and CD11b^{+} cells (pink). (A – D) Molecular (green M), Purkinje (green P), and
595 granular (green G) cell layers of the cerebellum and (C) POWV infected Purkinje cells (black
596 arrow). (E) CD11b positive cells (black arrow) around a vessel in the hippocampal region of a
597 DTV infected mouse brain. (H) Minimal infected cells (black arrow) in the hippocampal region of
598 a POWV infected mouse brain. (I) CD11b positive cells around a vessel (black arrow) and in the
599 leptomeninges (red arrow) of the isocortex of a DTV infected mouse brain. (K) CD11b positive
600 cells in the perivascular (Virchow-Robin) space (black arrow) of a POWV infected mouse brain.

601 **Fig. 6.** Severity of virus and CD11b in DTV and POWV-infected mouse brains by region. (A) Virus
602 severity individual mice by region and (B) brain regions of DTV infected mice had statistically
603 more virus severity in CTX, HPF, and TH while POWV infected mice had more virus severity in
604 CB. (C) CD11b severity of individual mice by region. (D) Brain regions of DTV infected mice had
605 statistically significant increases in CD11b positive cells in HPF. Comparisons performed using
606 unpaired two-tailed Student's t-test with Welch's correction.

607 **Fig. 7.** Divergent patterns of infection in DTV and POWV-infected mouse spinal cords.
608 Representative images of uninfected, DTV infected, and POWV infected mouse spinal cord with
609 teal staining of viral RNA and pink staining of neuronal nuclei (NeuN.) Uninfected cervical (A,
610 D), thoracic (G), and lumbar (J) regions with normal motor neurons shown (D, red arrows). DTV
611 infected mouse spinal cord cervical (B, E), thoracic (H), and lumbar (K) regions with minimal

612 infected neurons. POWV infected mouse spinal cord cervical (C, F), thoracic (I), and lumbar (L)
613 regions with decreasing infection across the cord and degenerating motor neurons (F, black
614 arrows.)

615 **Fig. 8.** RNA sequencing analysis of brain tissue. Brains were harvested at time of euthanasia
616 and stored in trizol before homogenization and RNA extraction followed by RNA-Seq.
617 Transcript libraries were analyzed using R with (A) POWV compared to DTV. Genes were
618 separated into smaller gene ontology sets and compared for (B) inflammatory response (C)
619 immune system process and (D) defense response.

620 **Fig. S1.** Comparison of differences between male and female mice infected with DTV or POWV.
621 Male (n = 6) and female (n = 6) DTV-infected mice had significantly different clinical observation
622 scores (A) on 7dpi at the AM observation [p = 0.0298] and changes to body weights (B) at 3dpi
623 [p = 0.04673]. No significant differences were found in survival (C), or viral RNA detected in
624 tissues (D) or blood (E). Male (n = 6) and female (n = 6) POWV-infected mice had significantly
625 different changes to body weights (G) at 4dpi [p = 0.03196] and differences in the amount of
626 viral RNA present in their livers (I) [p = 0.0257]. No significant differences were found in the
627 clinical observation scores (F), survival (H), or viral RNA present in the blood (J). Comparisons
628 were made using unpaired, two-tailed Student's t-test with Welch's correction. Error bars show
629 SEM.

630 **Fig. S2.** Cytokine and chemokine levels were measured in terminally collected serum from
631 uninfected (n = 6M/6F), DTV infected (n = 5M/6F), and POWV infected (n = 3M/5F) mice by Bio-
632 Plex Mouse Cytokine 23-plex panel. Significant differences were present between uninfected
633 and DTV-infected mice for six parameters (D, E, G, H, I, J), between uninfected and POWV-

634 infected mice for four parameters (A, B, C, F), and between DTV-and POWV infected mice for
635 one parameter (F). Comparisons were made using Brown-Forsythe and Welch's ANOVA test
636 with Dunnett's T3 multiple comparisons test.

637 **Fig. S3.** RNA sequencing analysis of brain tissue. Brains were harvested at moribundity and
638 stored in trizol before homogenization and RNA extraction followed by RNA-Seq. Transcript
639 libraries were analyzed using R with (A) POWV and (B) DTV compared to uninfected controls
640 and the 25 smallest adjusted p-values represented in a heat map for (C) POWV and (D) DTV.

641 **Fig. S4.** GO Term analysis of RNA sequencing from infected brain tissue. Transcripts from
642 previous RNA sequencing (Fig. 4, SI Appendix – Fig. S6) analyzed using Kyoto Encyclopedia of
643 Genes and Genomes (KEGG) using R for the top 25 overrepresented GO terms for (A) POWV
644 and (B) DTV compared to uninfected controls and (C) POWV compared to DTV.

645 **Table S1.** Clinical observation categories and scores. The highest scoring observation within a
646 category determined the score for the category. Scores from each category were added to
647 determine the total score.

648 **Table S2.** Distribution and severity of histologic lesions in brains. H&E-stained brain sections
649 were assessed for microscopic lesions including microgliosis (MG), perivascular cuffing (PC), and
650 neuronal necrosis (NN). Semi-quantitative scoring is indicated by 0 (absence of lesions), 1 (very
651 few to low), 2 (moderate), and 3 (numerous). Meningitis (M), encephalitis (E), and
652 meningoencephalitis (ME) were also noted. Areas that were not present were noted as NP.

653 **Table S3.** Presence of viral RNA and CD11b in the brain via RNAscope. Staining for viral RNA
654 (teal) and CD11b (pink) was performed using RNAscope. Brain regions were semi-quantitatively

655 scored with 0 (absence of staining), 1 (very few to low), 2 (moderate), and 3 (numerous).

656 Meningitis (M), encephalitis (E), and meningoencephalitis (ME) were also noted. Areas that

657 were not present were noted as NP.

658 **Table S4.** RNA-Seq full list of comparisons by gene.

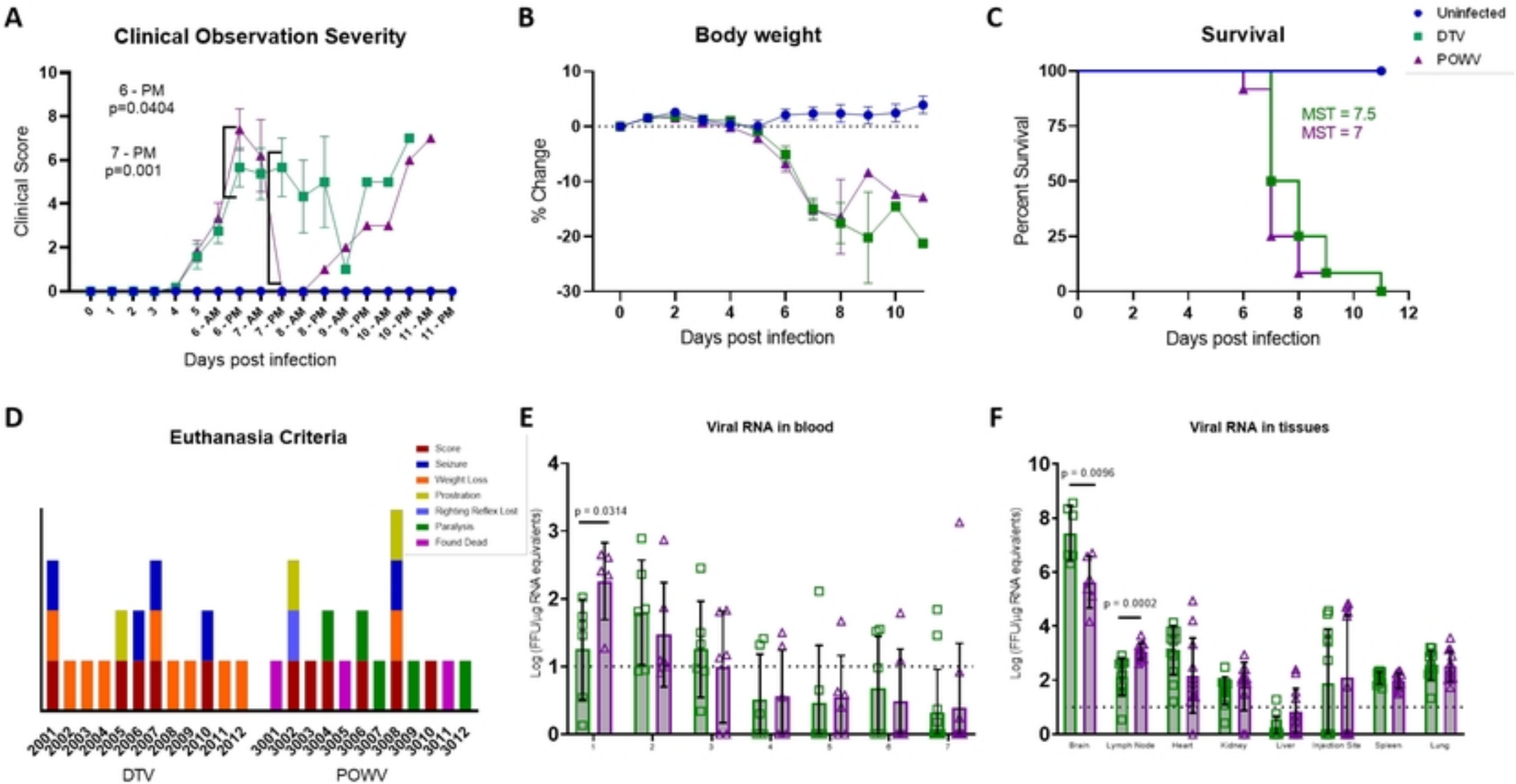
A
Clinical Observation Severity
6 - PM
p=0.0404
7 - PM
p=0.001
Clinical Score
Days post infection
B
Body weight
% Change
Days post infection
C
Survival
Uninfected
DTV
POWV
MST = 7.5
MST = 7
Percent Survival
Days post infection
D
Euthanasia Criteria
Score
Seizure
Weight Loss
Prostration
Righting Reflex Lost
Paralysis
Found Dead
DTV
POWV
E
Viral RNA in blood
p = 0.0314
Log (FFU/µg RNA equivalents)
F
Viral RNA in tissues
p = 0.0096
p = 0.0002
Log (FFU/µg RNA equivalents)
Brain
Lymph Node
Heart
Kidney
Liver
Injection Site
Spleen
Lung

Figure 1

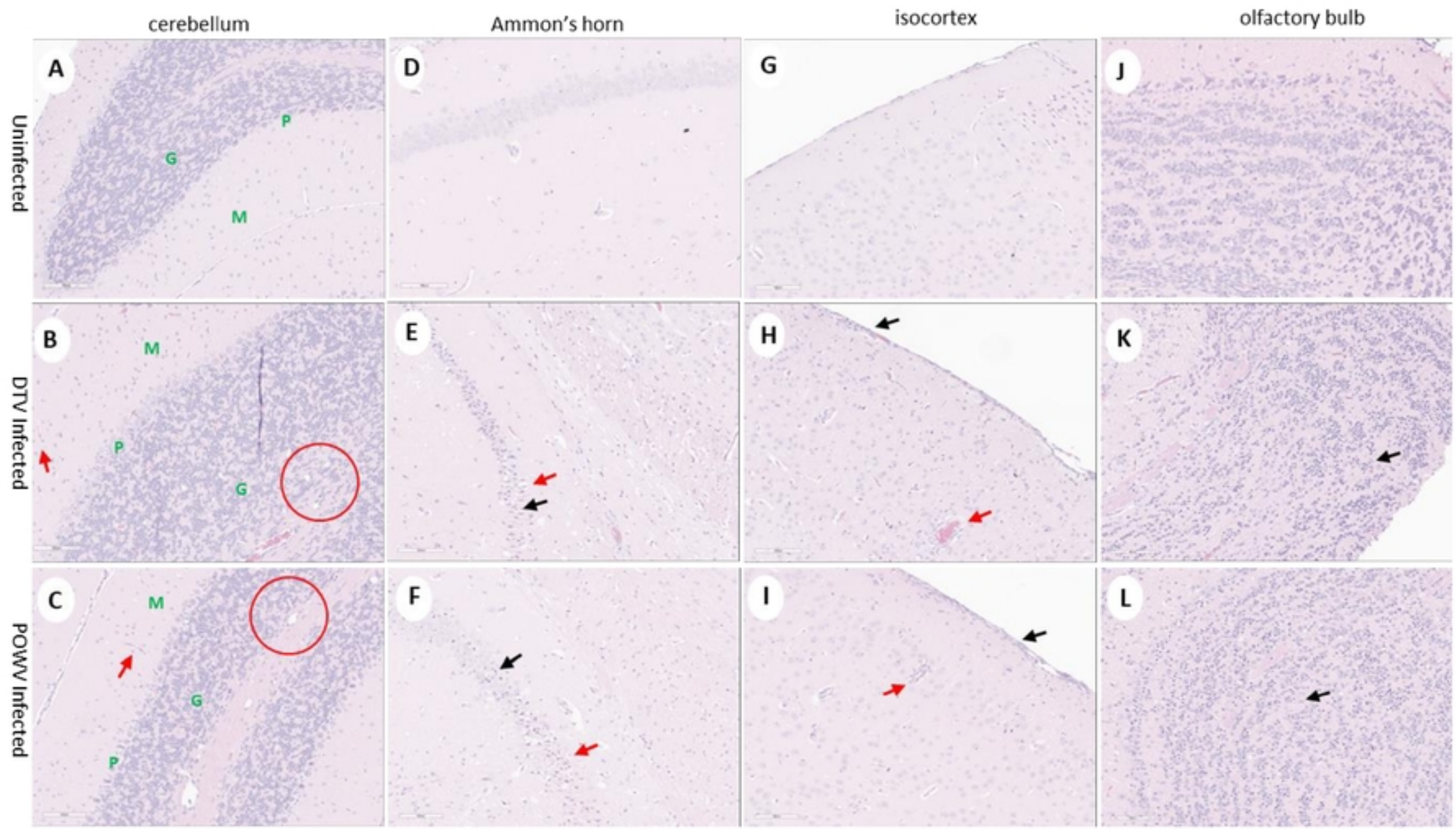
cerebellum
Ammon's horn
isocortex
olfactory bulb
Uninfected
DTV Infected
POWV Infected
A
B
C
D
E
F
G
H
I
J
K
L
P
G
M

Figure 2

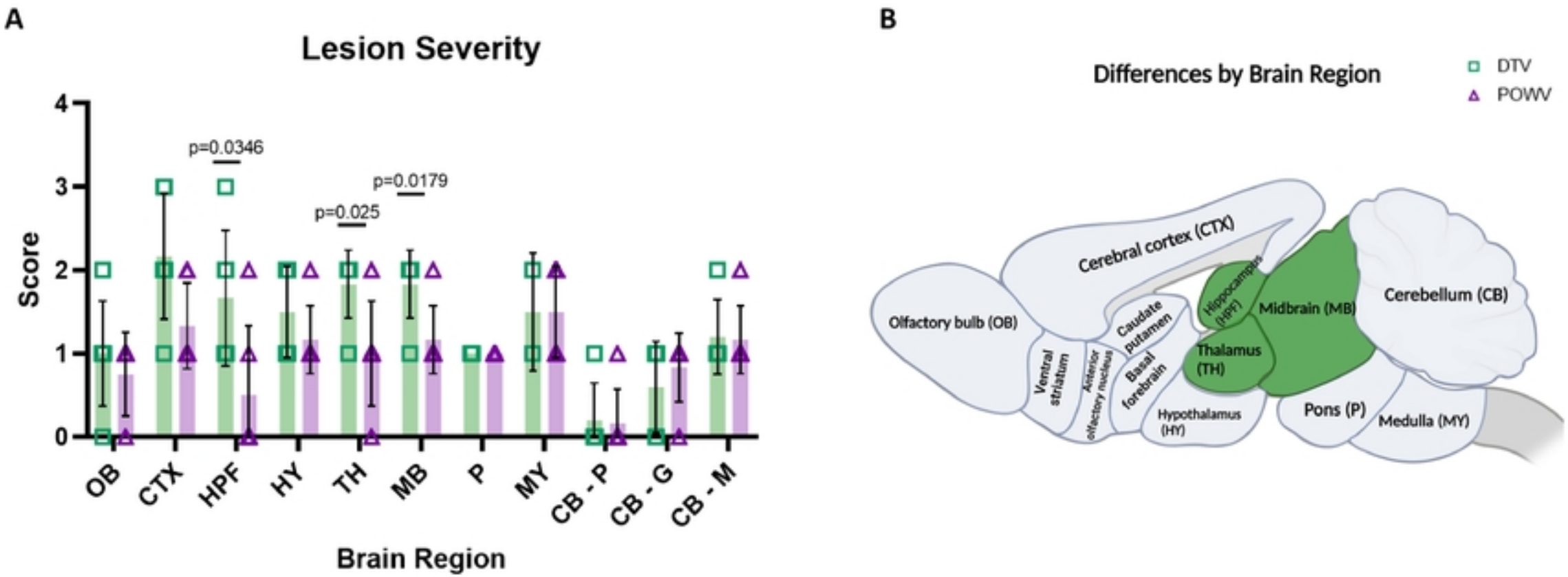
A
Lesion Severity
Score
4
3
2
1
0
p=0.0346
p=0.025
p=0.0179
OB
CTX
HPF
HY
TH
MB
P
MY
CB - P
CB - G
CB - M
Brain Region
B
Differences by Brain Region
DTV
POWV
Cerebral cortex (CTX)
Olfactory bulb (OB)
Hippocampus (HPF)
Midbrain (MB)
Cerebellum (CB)
Caudate putamen
Thalamus (TH)
Ventral striatum
Anterior olfactory nucleus
Basal forebrain
Hypothalamus (HY)
Pons (P)
Medulla (MY)

Figure 3

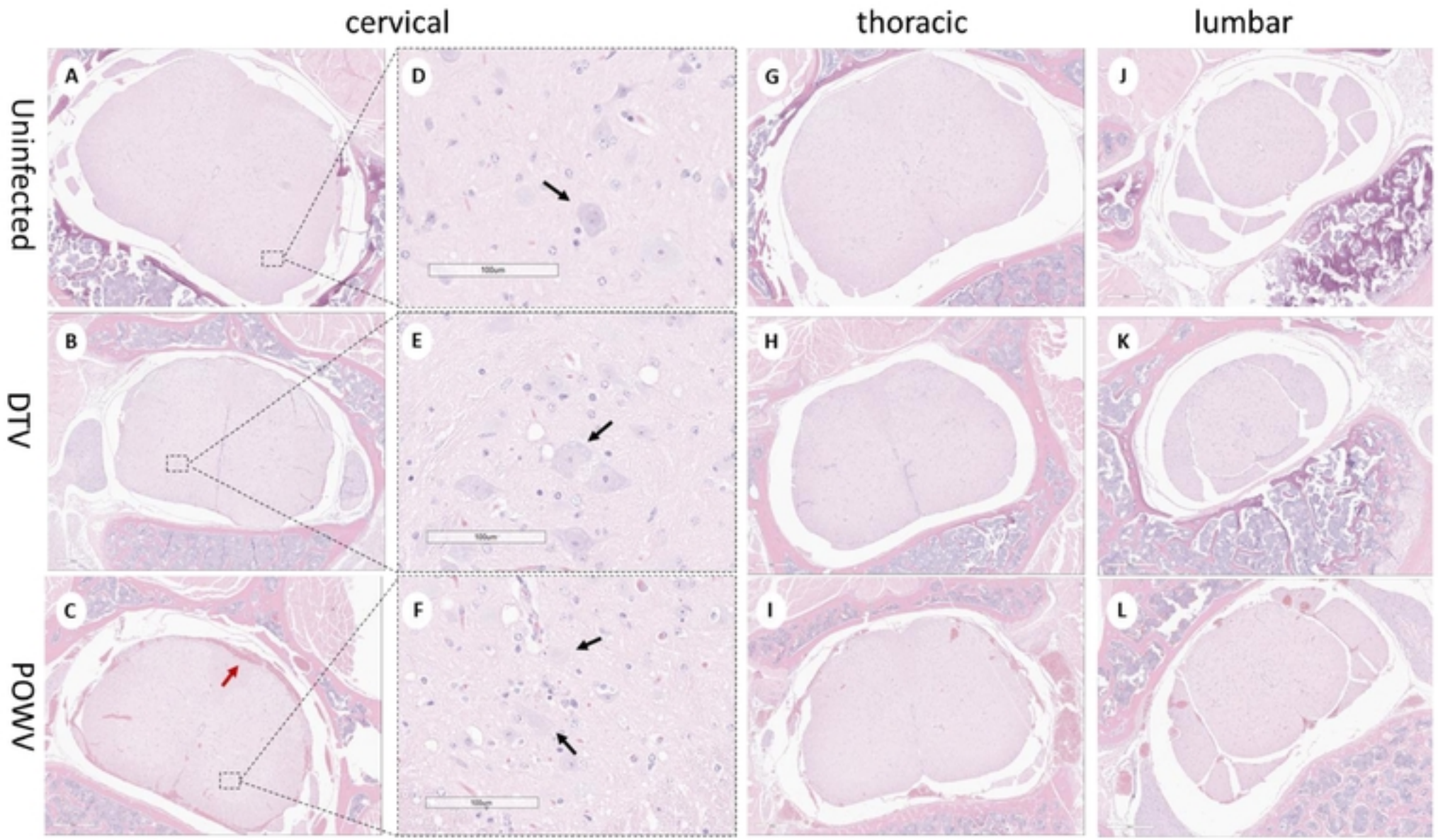
cervical
thoracic
lumbar
Uninfected
DTV
POWV
A
B
C
D
E
F
G
H
I
J
K
L

Figure 4

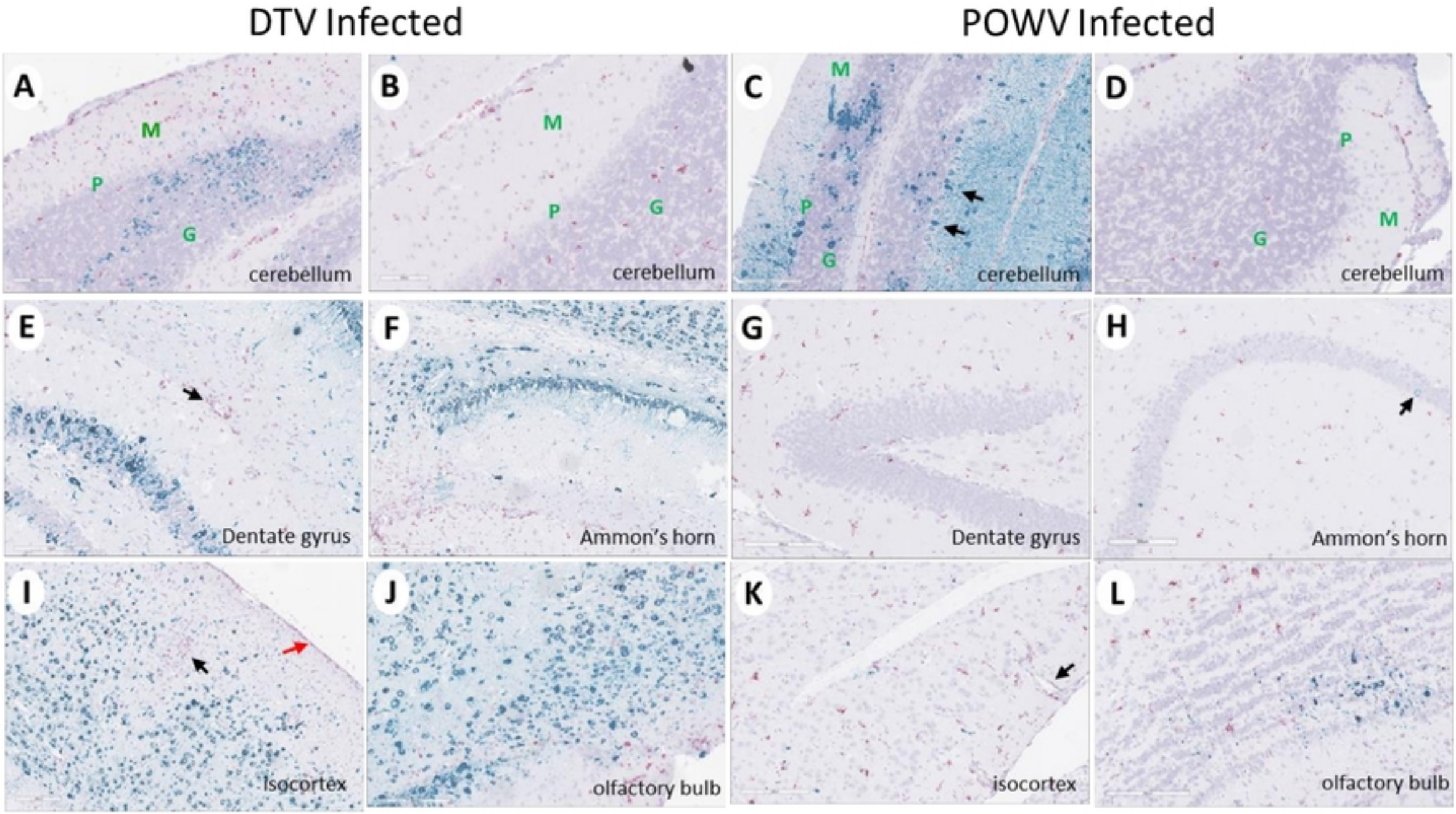
DTV Infected
POWV Infected
A
M
P
G
cerebellum
B
M
P
G
cerebellum
C
M
P
G
cerebellum
D
P
M
G
cerebellum
E
Dentate gyrus
F
Ammon's horn
G
Dentate gyrus
H
Ammon's horn
I
Isocortex
J
olfactory bulb
K
isocortex
L
olfactory bulb

Figure 5

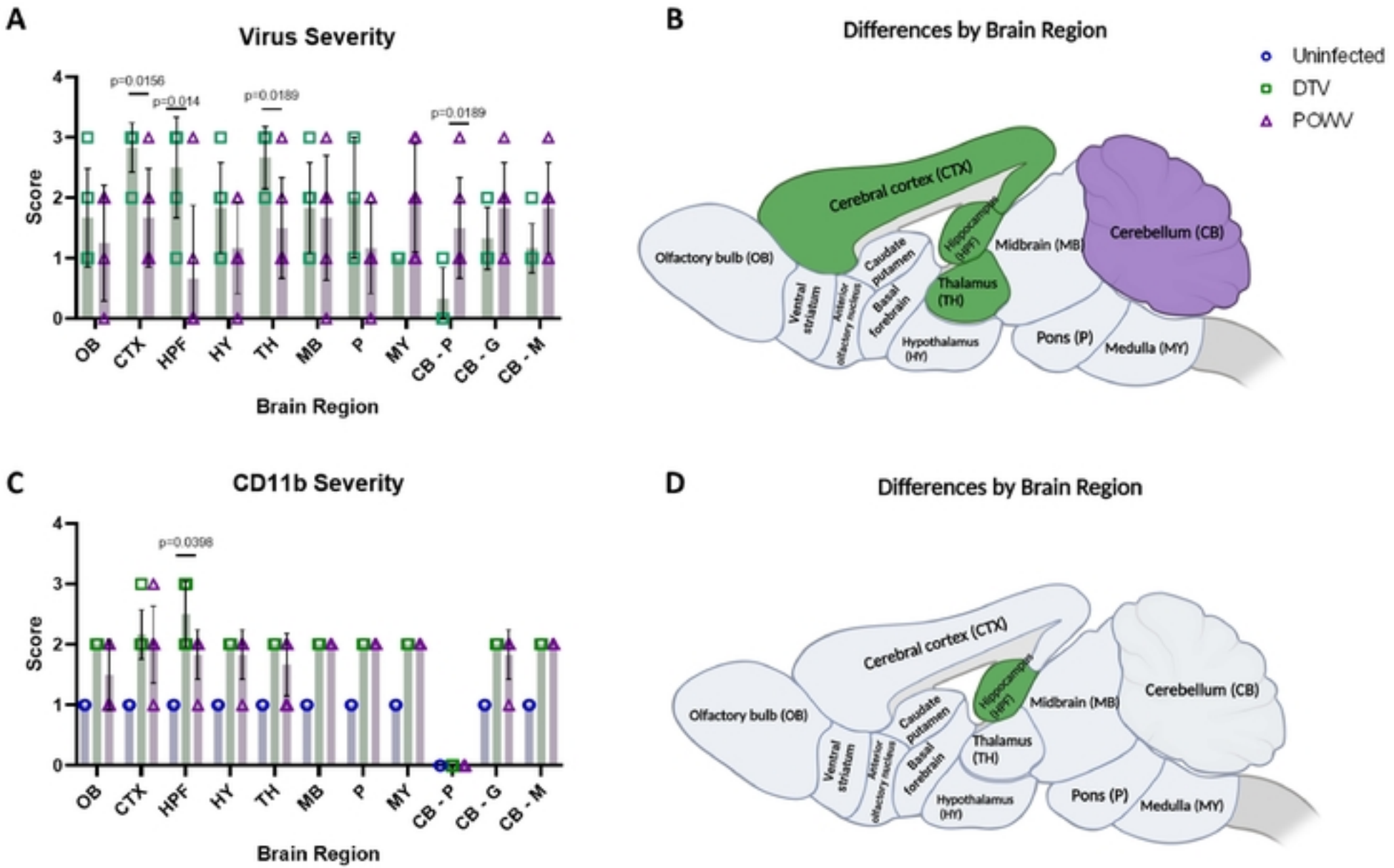
A
Virus Severity
Score
Brain Region
p=0.0156
p=0.014
p=0.0189
p=0.0189
OB
CTX
HPF
HY
TH
MB
P
MY
CB - P
CB - G
CB - M
B
Differences by Brain Region
Uninfected
DTV
POWV
Cerebral cortex (CTX)
Olfactory bulb (OB)
Caudate putamen
Hippocampus (HPF)
Midbrain (MB)
Cerebellum (CB)
Ventral striatum
Anterior olfactory nucleus
Basal forebrain
Thalamus (TH)
Hypothalamus (HY)
Pons (P)
Medulla (MY)
C
CD11b Severity
Score
Brain Region
p=0.0398
OB
CTX
HPF
HY
TH
MB
P
MY
CB - P
CB - G
CB - M
D
Differences by Brain Region
Cerebral cortex (CTX)
Olfactory bulb (OB)
Caudate putamen
Hippocampus (HPF)
Midbrain (MB)
Cerebellum (CB)
Ventral striatum
Anterior olfactory nucleus
Basal forebrain
Thalamus (TH)
Hypothalamus (HY)
Pons (P)
Medulla (MY)

Figure 6

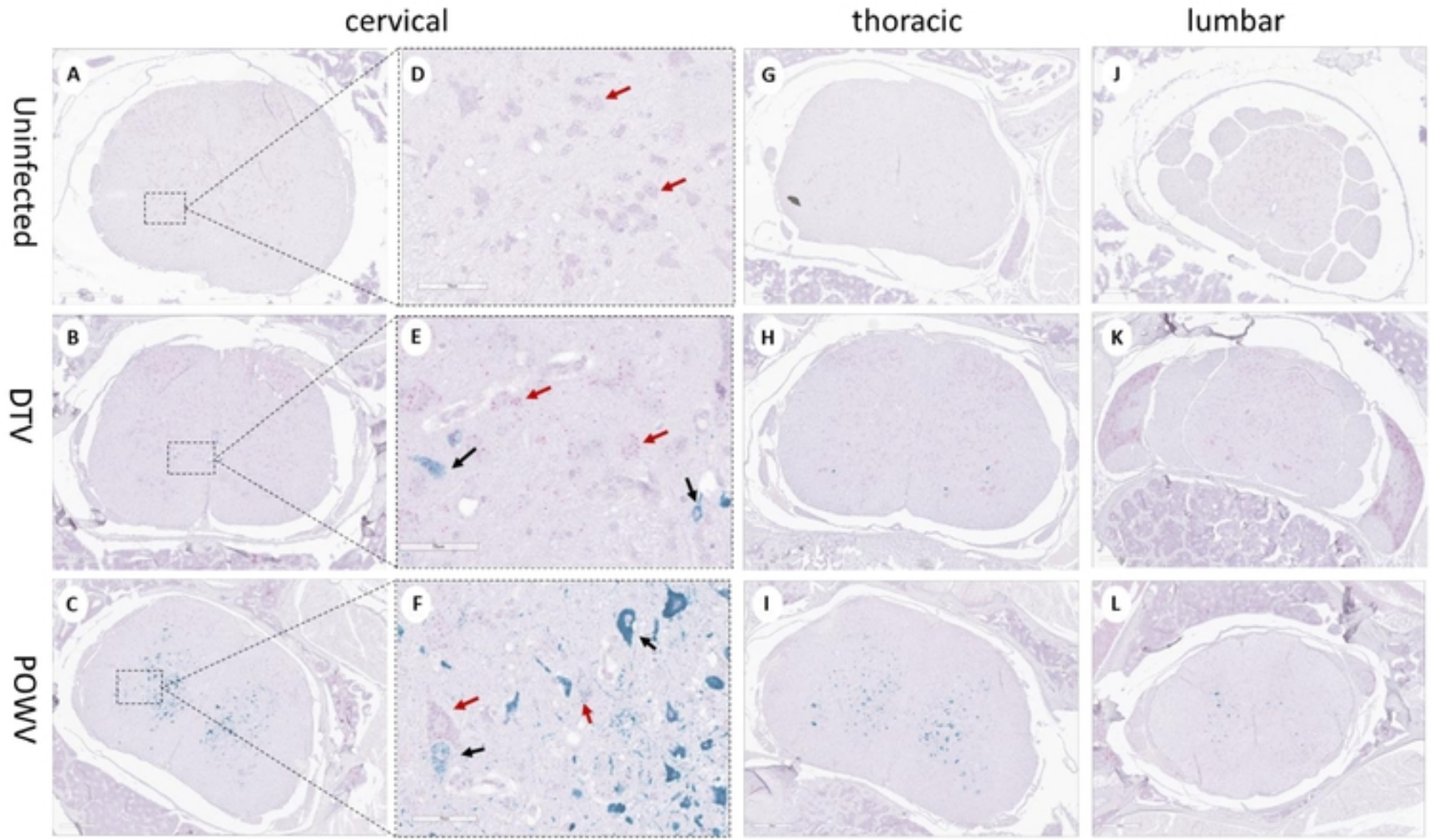
cervical
thoracic
lumbar
Uninfected
DTV
POWV
A
B
C
D
E
F
G
H
I
J
K
L

Figure 7

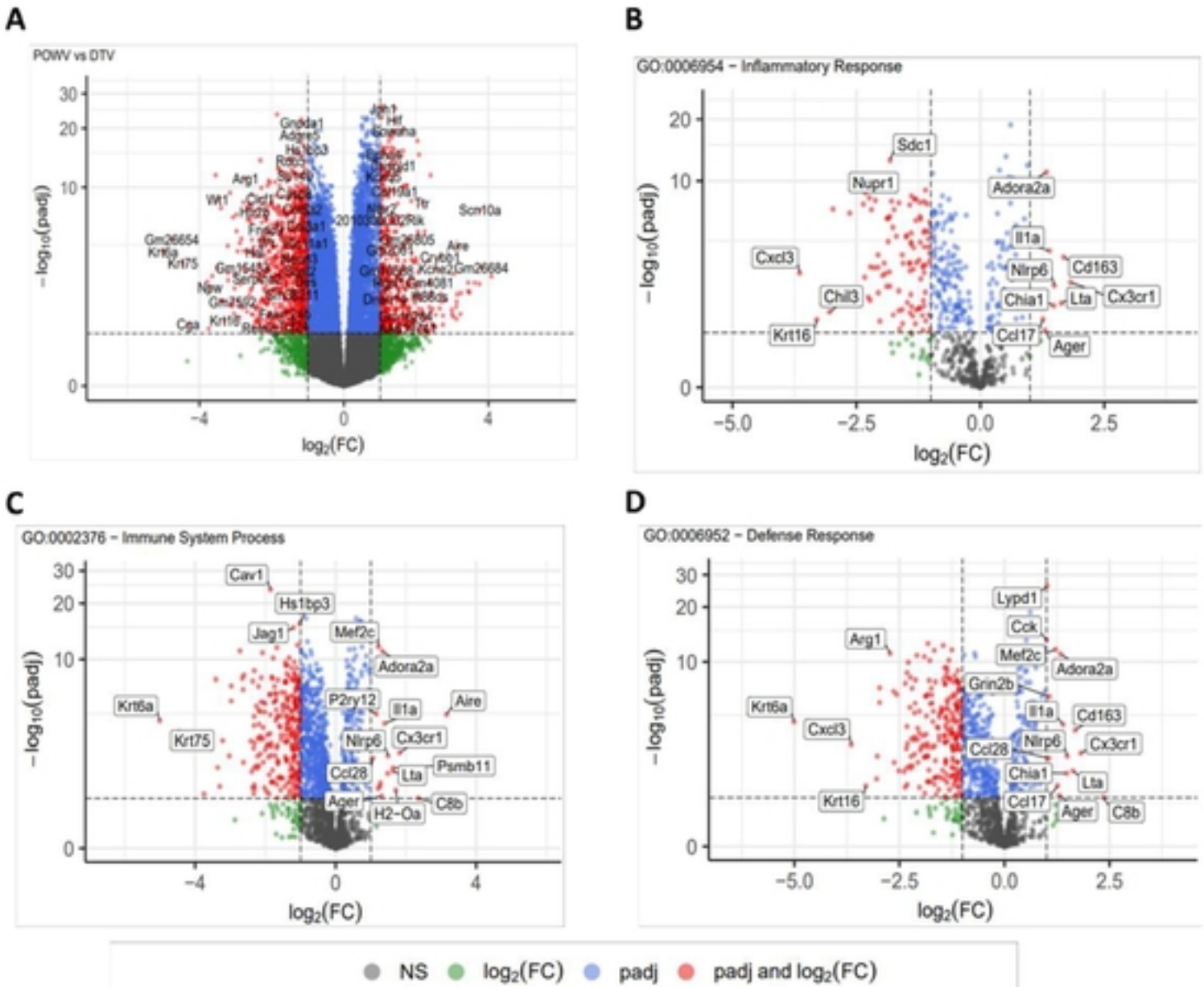
A
POWV vs DTV
B
GO:0006954 – Inflammatory Response
Sdc1
Nupr1
Adora2a
Il1a
Cxcl3
Nlrp6
Cd163
Chil3
Chia1
Lta
Cx3cr1
Krt16
Ccl17
Ager
C
GO:0002376 – Immune System Process
Cav1
Hs1bp3
Jag1
Mef2c
Adora2a
Krt6a
P2ry12
Il1a
Aire
Krt75
Nlrp6
Cx3cr1
Ccl28
Psmb11
Lta
Ager
C8b
H2-Oa
D
GO:0006952 – Defense Response
Lypd1
Cck
Arg1
Mef2c
Adora2a
Grin2b
Krt6a
Il1a
Cd163
Cxcl3
Nlrp6
Cx3cr1
Ccl28
Chia1
Lta
Krt16
Ccl17
Ager
C8b
$-\log_{10}(padj)$
$\log_2(FC)$
NS
$\log_2(FC)$
padj
padj and $\log_2(FC)$

Figure 8